# Quadrotor Fault-Tolerant Control at High Speed: A Model-Based Extended State Observer for Mismatched Disturbance Rejection Approach

Jinfeng Chen, Fan Zhang, *Graduate Student Member, IEEE*, Bin Hu, *Member, IEEE*, and Qin Lin, *Member, IEEE*

***Abstract*—Fault-tolerant control of a quadrotor in extreme conditions, such as rotor failure and strong winds, is exceptionally challenging due to its underactuated nature, strong mismatched disturbances, and highly nonlinear multi-input and multi-output properties. This letter proposes a reduced attitude control approach that combines a model-based extended state observer (MB-ESO) and mismatched disturbance decoupling to control a quadrotor under strong winds and complete loss of two opposing rotors. Our MB-ESO based control provides a new theoretical framework for more general nonlinear systems by utilizing all measurable outputs, thereby maximizing the use of all available information to design a robust controller. Testing in a high-fidelity simulator shows that our approach outperforms the state-of-the-art Incremental Nonlinear Dynamic Inversion method.**

***Index Terms*—Fault-tolerant control, flight control, extended state observer, mismatched disturbance rejection.**

## I. Introduction

MANY safety-critical and mission-critical quadrotors operate in highly uncertain and adverse environments, such as strong winds and the risk of rotor failures or attacks. These conditions pose significant challenges, particularly due to the complexities of modeling aerodynamics at high speeds and the lack of actuator redundancy.

Fault-tolerant control (FTC) has been studied to improve flight safety in the event of actuator failures [1], [2], [3], [4], [5], [6], [7]. The relaxed hover approach in [8] even studied the extreme case of three rotor failures. However, high-speed and aggressive maneuvers are rarely addressed in the literature. Most existing works focus on stationary environments at low speeds without significant disturbances.

Recently, incremental nonlinear dynamic inversion (INDI) control algorithms have emerged as promising solutions for quadrotors operating at high speeds with aggressive maneuvers [3], [4], [5], [6]. This approach utilizes sensor measurements and their derivatives to enhance robustness against model uncertainty and external disturbances.

Active disturbance rejection control (ADRC) [9] is similar to INDI in that it relies less on accurate model information. An extended state observer (ESO), an essential component in ADRC, estimates both the states and lumped disturbances, including internal disturbances caused by model uncertainty and external disturbances from the environment. A subsequent disturbance rejection controller can be designed accordingly once the disturbance has been estimated by the ESO. This method, following the separation principle, offers a superior modular design compared to direct robust methods such as the adaptive fuzzy approach [10]. There are several works on ADRC-based FTC [11], [12], however their focus is on stationary environments at low speeds.

Moreover, existing controllers based on ADRC typically require the original dynamic model to be divided into multiple SISO subsystems, which must have the form of cascades of integrators and matched disturbances. In this letter, we use the necessary and sufficient conditions for the existence of a model-based extended state observer (MB-ESO), as proposed in our recent work [13], as a criterion to design MB-ESOs for more general control-affine nonlinear systems subject to mismatched disturbances. This letter employs a disturbance decoupling controller design for multi-input, multi-output (MIMO) affine nonlinear systems with mismatched disturbances [14]. The idea of reduced attitude control is used to properly select controlled outputs [4] to ensure the stability of the zero dynamics of the quadrotor when two opposing rotors are available. Note that we use two opposing rotors as a case study to facilitate comparison with the state of the art [4]. By using reduced attitude for control output selection along with our general observer and controller design, it is straightforward to generalize to other cases, such as different numbers of missing rotors or two adjacent missing rotors.

Received 10 September 2024; revised 21 November 2024; accepted 8 December 2024. Date of publication 16 December 2024; date of current version 24 December 2024. This work was supported in part by the National Science Foundation under Grant 2301543. Recommended by Senior Editor L. Zhang. *(Corresponding author: Qin Lin.)*

Jinfeng Chen and Bin Hu are with the Department of Engineering Technology, University of Houston, Houston, TX 77004 USA (e-mail: particlefilter2012@gmail.com; bhu12@central.uh.edu).

Fan Zhang and Qin Lin are with the Department of Engineering Technology, and the Department of Electrical and Computer Engineering, University of Houston, Houston, TX 77004 USA (e-mail: fzhang28@cougarnet.uh.edu; qlin21@central.uh.edu).

Digital Object Identifier 10.1109/LCSYS.2024.3519033

2475-1456 © 2024 IEEE. All rights reserved, including rights for text and data mining, and training of artificial intelligence and similar technologies. Personal use is permitted, but republication/redistribution requires IEEE permission.
See https://www.ieee.org/publications/rights/index.html for more information.

Authorized licensed use limited to: University of Houston. Downloaded on February 18,2025 at 21:35:07 UTC from IEEE Xplore. Restrictions apply.

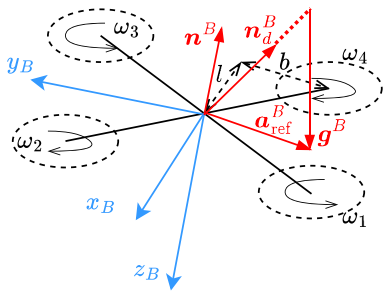


Fig. 1. Visualizations of quadrotor and reduced attitude.

The main contribution is the extension of our MB-ESO theory to a challenging quadrotor FTC within a new framework. (1) Unlike existing ESO-based controls that require stringent structural constraints, our new design has flexibility for a broader range of nonlinear systems. (2) It utilizes all available measured outputs and model information for observer design. (3) We integrate the MB-ESO with mismatched disturbance decoupling under the principle of reduced attitude, demonstrating superior robustness and tracking performance in strong winds compared to the INDI [4].

## II. Preliminary and Problem Formulation

*Notation:* Boldface symbols like $\boldsymbol{P}$ denote vectors or matrices, while non-boldface symbols like $p$ denote scalars. Superscripts $[\,\cdot\,]^I$ and $[\,\cdot\,]^B$ indicate coordinates expressed in the inertial and body frames, respectively. Subscripts specify relationships or attributes; *e.g.,* $\boldsymbol{x}_I$ represents the $x$-axis in the inertial frame. $0_{m\times n}$ denotes a $m$ by $n$ zero matrix and $\boldsymbol{I}_{m\times m}$ denotes an $m$-dimension identity matrix.

### A. Quadrotor Dynamic Model

Let $\mathcal{F}_{\mathcal{I}} = \{O_I, \boldsymbol{x}_I, \boldsymbol{y}_I, \boldsymbol{z}_I\}$ denote a right-hand inertial frame fixed to the ground, where $\boldsymbol{x}_I$, $\boldsymbol{y}_I$, and $\boldsymbol{z}_I$ point to the north, east, and points down, respectively. As shown in Fig. 1, $\mathcal{F}_{\mathcal{B}} = \{O_B, \boldsymbol{x}_B, \boldsymbol{y}_B, \boldsymbol{z}_B\}$ is a right-hand body frame fixed to the quadrotor with $O_B$ located at the center of mass, and $\boldsymbol{x}_B$, $\boldsymbol{y}_B$ and $\boldsymbol{z}_B$ pointing forward, right and down, respectively.

The complete dynamical model is as follows [4]:

$$\dot{\boldsymbol{P}}^I = \boldsymbol{V}^I \tag{1a}$$

$$m_v\dot{\boldsymbol{V}}^I = m_v\boldsymbol{g}^I + \boldsymbol{R}_{IB}\boldsymbol{F}^B \tag{1b}$$

$$\dot{\boldsymbol{R}}_{IB} = \boldsymbol{R}_{IB}\boldsymbol{\Omega}_{\times}^B \tag{1c}$$

$$\boldsymbol{I}_v\dot{\boldsymbol{\Omega}}^B = -\boldsymbol{\Omega}_{\times}^B\boldsymbol{I}_v\boldsymbol{\Omega}^B + \boldsymbol{M}^B \tag{1d}$$

where the translation dynamics are described in (1a) and (1b), and the rotation dynamics are described in (1c) and (1d); $\boldsymbol{P}^I = [X, Y, Z]^T$, $\boldsymbol{V}^I = [V_x, V_y, V_z]^T$, and $\boldsymbol{g}^I = [0, 0, g]^T$ are the position, velocity, and gravity vectors in $\mathcal{F}_{\mathcal{I}}$; $\boldsymbol{\Omega}^B = [p, q, r]^T$ is the angular velocity vector in $\mathcal{F}_{\mathcal{B}}$ including pitch rate, roll rate, and yaw rate; $\boldsymbol{R}_{IB}$ represents the rotation matrix from $\mathcal{F}_{\mathcal{B}}$ to $\mathcal{F}_{\mathcal{I}}$; $\boldsymbol{\Omega}_{\times}^B$ denotes the skew-symmetric matrix such that $\boldsymbol{\Omega}_{\times}^B\boldsymbol{a} = \boldsymbol{\Omega}^B \times \boldsymbol{a}$ for the vector cross product $\times$ and any vector $\boldsymbol{a} \in \mathbb{R}^3$; $m_v$ and $\boldsymbol{I}_v$ represent the gross mass and inertial matrix of the quadrotor. The resultant force $\boldsymbol{F}^B$ and moment $\boldsymbol{M}^B$ applied to the center of mass of the quadrotor in $\mathcal{F}_{\mathcal{B}}$ are modeled as:

$$\boldsymbol{F}^B = \begin{bmatrix} 0 \\ 0 \\ -\kappa_0\sum_{i=1}^4\omega_i^2 \end{bmatrix} + \boldsymbol{F}_a \tag{2}$$

$$\boldsymbol{M}^B = \begin{bmatrix} b\kappa_0 & -b\kappa_0 & -b\kappa_0 & b\kappa_0 \\ l\kappa_0 & l\kappa_0 & -l\kappa_0 & -l\kappa_0 \\ \tau_0 & -\tau_0 & \tau_0 & -\tau_0 \end{bmatrix}\begin{bmatrix} \omega_1^2 \\ \omega_2^2 \\ \omega_3^2 \\ \omega_4^2 \end{bmatrix} + \begin{bmatrix} 0 \\ 0 \\ -\gamma r \end{bmatrix} + \begin{bmatrix} I_p q(\omega_1 - \omega_2 + \omega_3 - \omega_4) \\ -I_p p(\omega_1 - \omega_2 + \omega_3 - \omega_4) \\ I_p(\dot{\omega}_1 - \dot{\omega}_2 + \dot{\omega}_3 - \dot{\omega}_4) \end{bmatrix} + \boldsymbol{M}_a \tag{3}$$

where $\kappa_0$ and $\tau_0$ are coefficients of the thrust and the reaction torque; $b$ and $l$ are geometric parameters of the quadrotor shown in Fig. 1; $\omega_i$ is the angular speed of the $i$th rotor rotating about the $z$ axis in $\mathcal{F}_{\mathcal{B}}$; $\gamma$ is the damping coefficient on yaw; $I_p$ represents the moment of inertial of each rotor inducing the gyroscopic moment; $\boldsymbol{F}_a$ and $\boldsymbol{M}_a$ are additional forces and torques caused by quadrotor model uncertainty, unmodeled aerodynamic effects and external wind.

### B. Reduced Attitude Control

Due to the inability to control the yaw angle in rotor failure cases, reduced attitude control [4], [8] simplifies the original attitude control to thrust vector pointing, compromising yaw control. $\boldsymbol{n}^B$ in Fig. 1 is a unit vector fixed to the body frame, as a rotation axis of the damaged quadrotor, and pointing in the same direction as the averaged thrust. To achieve position control, $\boldsymbol{n}^B$ must align with the reference unit vector $\boldsymbol{n}_d^B$, which is generated by the outer-loop controller for $\boldsymbol{n}_d^I$ in $\mathcal{F}_{\mathcal{I}}$ and subsequently converted to $\mathcal{F}_{\mathcal{B}}$. Eq. (1c) is replaced by the first two of the following relaxed attitude kinematic equations, as $\boldsymbol{n}_d^B$ is a unit vector with two independent components [4]:

$$\begin{bmatrix} \dot{h}_1 \\ \dot{h}_2 \\ \dot{h}_3 \end{bmatrix} = \begin{bmatrix} 0 & r & -q \\ -r & 0 & p \\ q & -p & 0 \end{bmatrix}\begin{bmatrix} h_1 \\ h_2 \\ h_3 \end{bmatrix} + \begin{bmatrix} \lambda_1 \\ \lambda_2 \\ \lambda_3 \end{bmatrix} \tag{4}$$

where $\boldsymbol{n}_d^B = [h_1, h_2, h_3]^T$, $\boldsymbol{R}_{IB}^T\dot{\boldsymbol{n}}_d^I = [\lambda_1, \lambda_2, \lambda_3]^T$ is a disturbance vector, and $\boldsymbol{n}_d^I$ is $\boldsymbol{n}_d^B$ expressed in $\mathcal{F}_{\mathcal{I}}$. For the quadrotor with two opposing rotors failure, $\boldsymbol{n}^B = [0, 0, -1]^T$ is chosen for the maximized energy efficiency. $h_1$ and $h_2$ should be both stabilized to zero to align $\boldsymbol{n}^B$ with $\boldsymbol{n}_d^B$.

### C. Problem Formulation

To illustrate the design of MB-ESO based control for the inner-loop controller more clearly, the dynamical model of the quadrotor after replacement can be written in the following affine nonlinear system with disturbance $\boldsymbol{w}$:

$$\begin{aligned} \dot{\boldsymbol{x}} &= \boldsymbol{f}(\boldsymbol{x}) + \boldsymbol{G}(\boldsymbol{x})\boldsymbol{u} + \boldsymbol{Q}(\boldsymbol{x})\boldsymbol{w} \\ \boldsymbol{y} &= \boldsymbol{H}(\boldsymbol{x}) \end{aligned} \tag{5}$$

where $\boldsymbol{x} = [Z, V_z, h_1, h_2, p, q, r]^T$, $\boldsymbol{u} = [\omega_1^2, \omega_2^2, \omega_3^2, \omega_4^2]^T$,

$$\boldsymbol{f}(\boldsymbol{x}) = \begin{bmatrix} V_z \\ g \\ h_2 r - h_3 q \\ -h_1 r + h_3 p \\ qr(I_y - I_z)/I_x \\ rp(I_z - I_x)/I_y \\ \big(-\gamma r + pq(I_x - I_y)\big)/I_z \end{bmatrix}, \tag{6}$$

Authorized licensed use limited to: University of Houston. Downloaded on February 18,2025 at 21:35:07 UTC from IEEE Xplore. Restrictions apply.

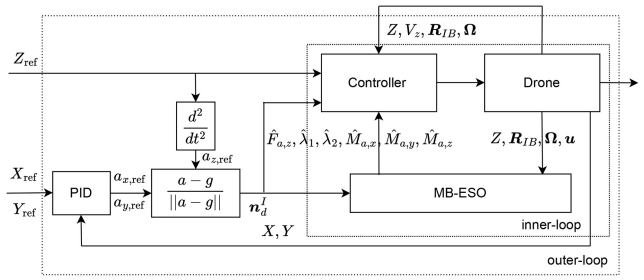


Fig. 2. Configuration of the cascaded control using PID as outer-loop position control and MB-ESO based control as inner-loop altitude/attitude control.

$$\boldsymbol{G}(\boldsymbol{x}) = \begin{bmatrix} 0 & 0 & 0 & 0 \\ -\frac{\kappa_0 R_{33}}{m_v} & -\frac{\kappa_0 R_{33}}{m_v} & -\frac{\kappa_0 R_{33}}{m_v} & -\frac{\kappa_0 R_{33}}{m_v} \\ 0 & 0 & 0 & 0 \\ 0 & 0 & 0 & 0 \\ \frac{b\kappa_0}{I_x} & -\frac{b\kappa_0}{I_x} & -\frac{b\kappa_0}{I_x} & \frac{b\kappa_0}{I_x} \\ \frac{l\kappa_0}{I_y} & \frac{l\kappa_0}{I_y} & -\frac{l\kappa_0}{I_y} & -\frac{l\kappa_0}{I_y} \\ \frac{\tau_0}{I_z} & -\frac{\tau_0}{I_z} & \frac{\tau_0}{I_z} & -\frac{\tau_0}{I_z} \end{bmatrix}, \tag{7}$$

$$\boldsymbol{Q}(\boldsymbol{x}) = \begin{bmatrix} 0_{1\times 6} \\ \boldsymbol{I}_{6\times 6} \end{bmatrix}, \tag{8}$$

$$\boldsymbol{H}(\boldsymbol{x}) = \begin{bmatrix} Z \\ h_1 \cos\chi + h_2 \sin\chi \end{bmatrix}, \tag{9}$$

$\boldsymbol{w} = [F_{a,z}, \lambda_1, \lambda_2, M_{a,x}, M_{a,y}, M_{a,z}]^T$ represents a disturbance vector in the inner-loop of the quadrotor, $\boldsymbol{I_v} = \text{diag}(I_x, I_y, I_z)$ is a diagonal inertia matrix, $R_{33}$ is the element at the third row and the third column of $\boldsymbol{R}_{IB}$, and the rotor induced gyroscopic moment is ignored. Every state can be measured or estimated. Since there remain two functional rotors, a maximum of two outputs can be controlled. The same outputs in [4] are used in (9), where the second output $y_2$ is the projection of $\boldsymbol{n}_d^B$ onto the axis $x$ of a new coordinate system obtained by rotating the body frame $\mathcal{F}_\mathcal{B}$ about $\boldsymbol{z}_B$ by an angle $\chi$. The zero dynamics of the quadrotor can be stabilized by properly selecting $\chi$, see [4] for more details. Without loss of generality, in this letter, we consider the case that rotors 2 and 4 remain functional, *i.e.*, $\omega_1^2$ and $\omega_3^2$ are assumed to be zero.

The research problem addressed in this letter is how to maximally exploit all available measured outputs and known model information to better estimate the disturbance $\boldsymbol{w}$, thereby improving control performance and robustness for the two-input, two-output affine nonlinear system (5).

## III. Proposed Framework

Fig. 2 shows a schematic overview of our framework, which consists of an outer-loop horizontal position controller and an inner-loop attitude and altitude controller.

### A. Controller Design for Outer-Loop Horizontal Position

To make a fair comparison with the INDI [4], our framework shares the same outer-loop PID controller generating desired rotation axis $\boldsymbol{n}_d^I$ in $\mathcal{F}_\mathcal{I}$, which can be obtained as

$$\boldsymbol{n}_d^I = \frac{\boldsymbol{a}_{\text{ref}}^I - \boldsymbol{g}^I}{||\boldsymbol{a}_{\text{ref}}^I - \boldsymbol{g}^I||} \tag{10}$$

where

$$\boldsymbol{a}_{\text{ref}}^I = \begin{bmatrix} -k_p e_x - k_d \dot{e}_x - k_i \int e_x dt \\ -k_p e_y - k_d \dot{e}_y - k_i \int e_y dt \\ \ddot{Z}_{\text{ref}} \end{bmatrix};$$

$e_x = X - X_{\text{ref}}$ and $e_y = Y - Y_{\text{ref}}$ are the horizontal position error in $\mathcal{F}_\mathcal{I}$; $k_p$, $k_i$, and $k_d$ are tunable PID parameters; $X_{\text{ref}}$, $Y_{\text{ref}}$, and $Z_{\text{ref}}$ represent the position of a reference trajectory.

### B. Controller Design for Inner-Loop Altitude and Attitude

*1) Design of MB-ESO:* The objective of designing the MB-ESO is to maximally exploit all available measured outputs and model information to estimate disturbances in the dynamic model. The sufficient and necessary conditions for the existence of an MB-ESO proposed in [13] are: 1) the system is observable, and 2) there is no invariant zero between the output and the disturbance. For system (5) with disturbance vector $\boldsymbol{w}$, the output vector for observers can be chosen as $\boldsymbol{y}_o = [Z, h_1, h_2, p, q, r]^T$. It can be easily verified that the system (5) with output $\boldsymbol{y}_o$ can be transferred in a normal form, with a disturbance vector relative degree of $\{2, 1, 1, 1, 1, 1\}$. The sum of these degrees is 7, which is equivalent to the number of states. Therefore, the system is observable and has no zero dynamics between $\boldsymbol{w}$ and $\boldsymbol{y}_o$ [15].

Reference [13] addresses only single-disturbance single-output (SDSO) linear systems, while the system in (5) is a multi-disturbance multi-output (MDMO) affine nonlinear system. To apply the results from [13], (5) is decomposed into six SDSO systems based on the disturbance vector relative degree, each containing a nonlinear term in the same channel as the disturbance. The disturbance vector $\boldsymbol{w}$ is treated as an extended state vector, enabling the design of six MB-ESOs:

$$\begin{bmatrix} \dot{\hat{Z}} \\ \dot{\hat{V}}_z \\ \dot{\hat{F}}_{a,z} \end{bmatrix} = \begin{bmatrix} -L_{1,1} & 1 & 0 \\ -L_{2,1} & 0 & 1 \\ -L_{3,1} & 0 & 0 \end{bmatrix} \begin{bmatrix} \hat{Z} \\ \hat{V}_z \\ \hat{F}_{a,z} \end{bmatrix} + \begin{bmatrix} 0_{1\times 4} \\ \boldsymbol{G}_2(\boldsymbol{x}) \\ 0_{1\times 4} \end{bmatrix} \boldsymbol{u} + \begin{bmatrix} 0 \\ f_2(\boldsymbol{x}) \\ 0 \end{bmatrix} + \begin{bmatrix} L_{1,1} \\ L_{2,1} \\ L_{3,1} \end{bmatrix} Z, \tag{11}$$

$$\begin{bmatrix} \dot{\hat{h}}_1 \\ \dot{\hat{\lambda}}_1 \end{bmatrix} = \begin{bmatrix} -L_{1,2} & 1 \\ -L_{2,2} & 0 \end{bmatrix} \begin{bmatrix} \hat{h}_1 \\ \hat{\lambda}_1 \end{bmatrix} + \begin{bmatrix} f_3(\boldsymbol{x}) \\ 0 \end{bmatrix} + \begin{bmatrix} L_{1,2} \\ L_{2,2} \end{bmatrix} h_1, \tag{12}$$

$$\begin{bmatrix} \dot{\hat{h}}_2 \\ \dot{\hat{\lambda}}_2 \end{bmatrix} = \begin{bmatrix} -L_{1,3} & 1 \\ -L_{2,3} & 0 \end{bmatrix} \begin{bmatrix} \hat{h}_2 \\ \hat{\lambda}_2 \end{bmatrix} + \begin{bmatrix} f_4(\boldsymbol{x}) \\ 0 \end{bmatrix} + \begin{bmatrix} L_{1,3} \\ L_{2,3} \end{bmatrix} h_2, \tag{13}$$

$$\begin{bmatrix} \dot{\hat{p}} \\ \dot{\hat{M}}_{a,x} \end{bmatrix} = \begin{bmatrix} -L_{1,4} & 1 \\ -L_{2,4} & 0 \end{bmatrix} \begin{bmatrix} \hat{p} \\ \hat{M}_{a,x} \end{bmatrix} + \begin{bmatrix} \boldsymbol{G}_5(\boldsymbol{x}) \\ 0_{1\times 4} \end{bmatrix} \boldsymbol{u} + \begin{bmatrix} f_5(\boldsymbol{x}) \\ 0 \end{bmatrix} + \begin{bmatrix} L_{1,4} \\ L_{2,4} \end{bmatrix} p, \tag{14}$$

$$\begin{bmatrix} \dot{\hat{q}} \\ \dot{\hat{M}}_{a,y} \end{bmatrix} = \begin{bmatrix} -L_{1,5} & 1 \\ -L_{2,5} & 0 \end{bmatrix} \begin{bmatrix} \hat{q} \\ \hat{M}_{a,y} \end{bmatrix} + \begin{bmatrix} \boldsymbol{G}_6(\boldsymbol{x}) \\ 0_{1\times 4} \end{bmatrix} \boldsymbol{u} + \begin{bmatrix} f_6(\boldsymbol{x}) \\ 0 \end{bmatrix} + \begin{bmatrix} L_{1,5} \\ L_{2,5} \end{bmatrix} q, \tag{15}$$

$$\begin{bmatrix} \dot{\hat{r}} \\ \dot{\hat{M}}_{a,z} \end{bmatrix} = \begin{bmatrix} -L_{1,6} & 1 \\ -L_{2,6} & 0 \end{bmatrix} \begin{bmatrix} \hat{r} \\ \hat{M}_{a,z} \end{bmatrix} + \begin{bmatrix} \boldsymbol{G}_7(\boldsymbol{x}) \\ 0_{1\times 4} \end{bmatrix} \boldsymbol{u}$$

Authorized licensed use limited to: University of Houston. Downloaded on February 18,2025 at 21:35:07 UTC from IEEE Xplore. Restrictions apply.

$$+\begin{bmatrix}\boldsymbol{f}_7(\boldsymbol{x})\\0\end{bmatrix}+\begin{bmatrix}L_{1,6}\\L_{2,6}\end{bmatrix}r, \tag{16}$$

where $\hat{Z}$, $\hat{V}_z$, $\hat{h}_1$, $\hat{h}_2$, $\hat{p}$, $\hat{q}$, $\hat{r}$, $\hat{F}_{a,z}$, $\hat{\lambda}_1$, $\hat{\lambda}_2$, $\hat{M}_{a,x}$, $\hat{M}_{a,y}$, and $\hat{M}_{a,z}$ are estimates; $\boldsymbol{G}_i(\boldsymbol{x})$ is the $i$th row of $\boldsymbol{G}(\boldsymbol{x})$ for $i=1,\ldots,7$; $\boldsymbol{f}_i(\boldsymbol{x})$ is the $i$th row of $\boldsymbol{f}(\boldsymbol{x})$ for $i=1,\ldots,7$; $L_{i,j}$ is the $i$th tunable observer gain for the $j$th MB-ESO for $i=1,\ldots,3$ and $j=1,\ldots,6$, which can be determined by the place of eigenvalues of MB-ESO. For simplicity, the eigenvalues of the $i$th MB-ESO are all placed at $-\nu_{oi}$, where $\nu_{oi}$ is the observer bandwidth of ESO [16].

*Remark 1:* Although [13] mainly considers discrete-time systems, it also generalizes to the case of continuous-time systems proposed in [17].

Next, we will show that the error dynamics of the MB-ESOs proposed for system (5) are the same as those in [13], [17]. For simplicity, we will use the MB-ESO described in (11) as an example. The augmented component of system (5) corresponding to (11) is

$$\begin{bmatrix}\dot{Z}\\\dot{V}_z\\\dot{F}_{a,z}\end{bmatrix}=\begin{bmatrix}0&1&0\\0&0&1\\0&0&0\end{bmatrix}\begin{bmatrix}Z\\V_z\\F_{a,z}\end{bmatrix}+\begin{bmatrix}0_{1\times4}\\\boldsymbol{G}_2(\boldsymbol{x})\\0_{1\times4}\end{bmatrix}\boldsymbol{u}+\begin{bmatrix}0\\\boldsymbol{f}_2(\boldsymbol{x})\\0\end{bmatrix}+\begin{bmatrix}0\\0\\1\end{bmatrix}\dot{F}_{a,z}. \tag{17}$$

Subtracting (11) from (17) yields the error dynamics:

$$\dot{\boldsymbol{e}}=(\boldsymbol{A}_o-\boldsymbol{L}\boldsymbol{C}_o)\boldsymbol{e}+\boldsymbol{E}_o\dot{F}_{a,z}, \tag{18}$$

where

$$\boldsymbol{e}=\begin{bmatrix}Z-\hat{Z}\\V_z-\hat{V}_z\\F_{a,z}-\hat{F}_{a,z}\end{bmatrix},\boldsymbol{A}_o=\begin{bmatrix}0&1&0\\0&0&1\\0&0&0\end{bmatrix},\boldsymbol{L}=\begin{bmatrix}L_{1,1}\\L_{2,1}\\L_{3,1}\end{bmatrix},$$

$\boldsymbol{C}_o=[1,0,0]$, and $\boldsymbol{E}_o=[0,0,1]^T$. Therefore, we verify that the condition in [13] holds for this system, and by applying pole placement to the observer, we can guarantee the convergence of disturbance estimation.

Reference [13] examines the connection between the MB-ESO and the unknown input observer (UIO), also known as the disturbance decoupled observer [18]. Established UIO theory supports MB-ESO development. Reference [19] proves geometrically that the number of decoupled disturbances in an observer cannot exceed the number of measured outputs. In this letter, the number of disturbances equals the number of measured outputs, ensuring maximal utilization of measurements for disturbance estimation in the MB-ESOs.

*2) Control Design for Mismatched Disturbances:* To design a control law $\boldsymbol{u}$ that makes the system output $\boldsymbol{y}$ follow the reference trajectory $[Z_{\text{ref}}, h_{1,\text{ref}}\cos\chi+h_{2,\text{ref}}\sin\chi]^T$, the effects of disturbance $\boldsymbol{w}$ on system (5) should be eliminated from $\boldsymbol{y}$. However, $\boldsymbol{w}$ cannot be canceled out directly in the input channel since $\boldsymbol{w}$ is not in the same channel as the control input $\boldsymbol{u}$, making $\boldsymbol{w}$ mismatched disturbances. The disturbance decoupling method proposed in [14] is adopted in this letter to reject mismatched disturbances.

The system (5) is converted into the normal form via a coordinate transformation $\boldsymbol{\Phi}(\boldsymbol{x})=\left[\boldsymbol{\eta},\boldsymbol{\xi}\right]^T$ [15], where $\boldsymbol{\eta}$ represents the states of the zero dynamics, see [4],

$$\begin{aligned}\boldsymbol{\xi}&=[\xi_1,\xi_2,\xi_3,\xi_4]^T\\&=\left[H_1(\boldsymbol{x}),L_fH_1(\boldsymbol{x}),H_2(\boldsymbol{x}),L_fH_2(\boldsymbol{x})\right]^T,\end{aligned} \tag{19}$$

$H_i(\boldsymbol{x})$ denotes the $i$th real-valued function in the vector field $\boldsymbol{H}(\boldsymbol{x})$, and $L_fH_i(\boldsymbol{x})$ is the first order Lie derivative of $H_i(\boldsymbol{x})$ along the vector field $\boldsymbol{f}(\boldsymbol{x})$. Since the zero dynamics of system (5) can be stabilized by properly selecting $\chi$ and control input $\boldsymbol{u}$ cannot change the place of zeros, the following subsystem under the new coordinates $\boldsymbol{\Phi}(\boldsymbol{x})$ without zero dynamics is used to design the control law:

$$\begin{aligned}\dot{\boldsymbol{\xi}}&=\boldsymbol{A}_c\boldsymbol{\xi}+\boldsymbol{B}_c[\boldsymbol{\alpha}(\boldsymbol{x})+\boldsymbol{\mathcal{B}}(\boldsymbol{x})u]+\boldsymbol{D}_c(\boldsymbol{x})\boldsymbol{w}\\\boldsymbol{y}&=\boldsymbol{C}_c\boldsymbol{\xi}\end{aligned} \tag{20}$$

where

$$\boldsymbol{A}_c=\begin{bmatrix}0&1&0&0\\0&0&0&0\\0&0&0&1\\0&0&0&0\end{bmatrix},\boldsymbol{B}_c=\begin{bmatrix}0&0\\1&0\\0&0\\0&1\end{bmatrix},\boldsymbol{C}_c=\begin{bmatrix}1&0\\0&0\\0&1\\0&0\end{bmatrix}^T,$$

$$\boldsymbol{D}_c(\boldsymbol{x})=\begin{bmatrix}L_{Q_1}H_1&L_{Q_2}H_1&\cdots&L_{Q_6}H_1\\L_{Q_1}L_fH_1&L_{Q_2}L_fH_1&\cdots&L_{Q_6}L_fH_1\\L_{Q_1}H_2&L_{Q_2}H_2&\cdots&L_{Q_6}H_2\\L_{Q_1}L_fH_2&L_{Q_2}L_fH_2&\cdots&L_{Q_6}L_fH_2\end{bmatrix},$$

$$\boldsymbol{\alpha}(\boldsymbol{x})=\begin{bmatrix}L_f^2H_1\\L_f^2H_2\end{bmatrix},\boldsymbol{\mathcal{B}}(\boldsymbol{x})=\begin{bmatrix}L_{G_2}L_fH_1&L_{G_4}L_fH_1\\L_{G_2}L_fH_2&L_{G_4}L_fH_2\end{bmatrix},$$

$u=[\omega_2^2,\omega_4^2]^T$ are the inputs of functional rotors 2 and 4, $Q_i$ is the $i$th column of $\boldsymbol{Q}(\boldsymbol{x})$, $G_i$ is the $i$th column of $\boldsymbol{G}(\boldsymbol{x})$, $L_{Q_j}L_fH_i$ is the first order Lie derivative of $H_i(\boldsymbol{x})$ first along the vector field $\boldsymbol{f}(\boldsymbol{x})$ and then along the vector filed $Q_j(\boldsymbol{x})$, $L_f^2H_i$ is the second order Lie derivative of $H_i(\boldsymbol{x})$ along the vector field $\boldsymbol{f}(\boldsymbol{x})$.

Since there exists a disturbance term $\boldsymbol{D}_c(\boldsymbol{x})\boldsymbol{w}$ in the system (20), a disturbance decoupling control law to compensate for the disturbances in the outputs $\boldsymbol{y}$ in steady state is given in the following [14]:

$$u=\boldsymbol{\mathcal{B}}^{-1}(\boldsymbol{x})[-\boldsymbol{\alpha}(\boldsymbol{x})+u_0+\boldsymbol{\Gamma}(\boldsymbol{x})\boldsymbol{w}] \tag{21}$$

where

$$\boldsymbol{\Gamma}(\boldsymbol{x})=\begin{bmatrix}\gamma_{11}(\boldsymbol{x})&\gamma_{12}(\boldsymbol{x})&\cdots&\gamma_{16}(\boldsymbol{x})\\\gamma_{21}(\boldsymbol{x})&\gamma_{22}(\boldsymbol{x})&\cdots&\gamma_{26}(\boldsymbol{x})\end{bmatrix},$$

$u_0=\left[-c_1^1(\xi_1-Z_{\text{ref}})-c_2^1\xi_2\quad -c_1^2\xi_3-c_2^2\xi_4\right]^T$, $\boldsymbol{\Gamma}(\boldsymbol{x})$ is determined such that the effects of $\boldsymbol{w}$ are eliminated in the output channels in steady state, and $c_1^i$ and $c_2^i$ can be calculated by placing all poles of the $i$th feedback loop at $-\nu_{ci}$, where $\nu_{ci}$ is called the controller bandwidth [16].

For simplicity, the first subsystem is used to illustrate how to derive the first row of $\boldsymbol{\Gamma}(\boldsymbol{x})$. Substituting (21) into (20), the first subsystem can be written as

$$\begin{aligned}\begin{bmatrix}\dot{\xi}_1\\\dot{\xi}_2\end{bmatrix}&=\begin{bmatrix}0&1\\-c_1^1&-c_2^1\end{bmatrix}\begin{bmatrix}\xi_1\\\xi_2\end{bmatrix}+\begin{bmatrix}0\\1\end{bmatrix}c_1^1Z_{\text{ref}}\\&\quad+\begin{bmatrix}\sum_{i=1}^6L_{Q_i}H_1w_i\\\sum_{i=1}^6L_{Q_i}L_fH_1w_i\end{bmatrix}+\begin{bmatrix}0\\\sum_{i=1}^6\gamma_{1i}w_i\end{bmatrix}\\y_1&=\begin{bmatrix}1&0\end{bmatrix}\begin{bmatrix}\xi_1\\\xi_2\end{bmatrix}.\end{aligned} \tag{22}$$

Authorized licensed use limited to: University of Houston. Downloaded on February 18,2025 at 21:35:07 UTC from IEEE Xplore. Restrictions apply.

TABLE I
PARAMETERS OF THE QUADROTOR

| Parameters | Values | Parameters | Values |
|---|---|---|---|
| $I_x$ | $1.4e^{-3}$ kg·m$^2$ | $m_v$ | 0.375 kg |
| $I_y$ | $1.3e^{-3}$ kg·m$^2$ | $b$ | 0.115 m |
| $I_z$ | $2.5e^{-3}$ kg·m$^2$ | $l$ | 0.0875 m |
| $\kappa_0$ | $1.9e^{-6}$ kg·m/rad$^2$ | $g$ | 9.81 m/s$^2$ |
| $\tau_0$ | $1.9e^{-8}$ kg·m$^2$/rad$^2$ | $\gamma$ | $1.92e^{-3}$ N·m·s |
| $\chi$ | 75 degree | | |

TABLE II
CONTROL PARAMETERS OF THE MB-ESO BASED CONTROL

| MB-ESO | | | | | | |
|---|---|---|---|---|---|---|
| index | 1 | 2 | 3 | 4 | 5 | 6 |
| bandwidth [rad/s] | 12 | 140 | 140 | 140 | 140 | 140 |
| Inner-loop Controller | | | | | | |
| index | 1 | 2 | | | | |
| bandwidth [rad/s] | 5 | 11 | | | | |
| Outer-loop Controller | | | | | | |
| | $k_{p,x}$ | $k_{p,y}$ | $k_{p,z}$ | $k_{d,x}$ | $k_{d,y}$ | $k_{d,z}$ |
| | 1 | 1 | 10 | 2 | 2 | 6 |
| | $k_{i,x}$ | $k_{i,y}$ | $k_{i,z}$ | | | |
| | 0 | 0 | 0 | | | |

The last two terms in (22) should have zero impact on the output $y_1$ in steady state, which can be formulated as

$$\begin{bmatrix}1 & 0\end{bmatrix}\begin{bmatrix}0 & 1\\ -c_1^1 & -c_2^1\end{bmatrix}^{-1}\begin{bmatrix}\sum_{i=1}^{6} L_{Q_i}H_1 w_i\\ \sum_{i=1}^{6}\left(L_{Q_i}L_f H_1+\gamma_{1i}\right)w_i\end{bmatrix}=0. \quad (23)$$

Solving (23) for $\gamma_{1i}$ yields

$$\gamma_{1i}=-L_{Q_i}L_f H_1-c_2^1 L_{Q_i}H_1 \quad \forall i=1,\ldots,6. \quad (24)$$

## IV. SIMULATION RESULTS

To make a fair comparison between our approach and the notable INDI fault-tolerant control [4], we use the same open-source simulator[1] developed by the authors. The parameters of the quadrotor in Table I are used in the designs of the INDI and ours. The maximum tilt angle of the quadrotor is set to 30 degrees. The angular speed range of each rotor lies in 0 rad/s to 1200 rad/s. We use the same noise settings as [4], with power values of $1\times10^{-8}$, $1\times10^{-8}$, $2\times10^{-4}$, and $1\times10^{-5}$ applied to position, attitude, angular velocity, and rotor speed measurements, respectively, using Band-Limited White Noise in Simulink®. The observer bandwidths and control bandwidths in the inner-loop and the PID gains in the outer-loop for the proposed control method are given in Table II. The control gains in the inner-loop for the INDI method are given in Table III with the same outer-loop parameters.

Fig. 3(a) shows that the tracking performances on the $X$ axis for ours and INDI are similar without any over-shooting. However, due to aggressive maneuvering and significant unmodeled aerodynamics, substantial fluctuations occur on the $Y$ and $Z$ axes and $y_2$ when the quadrotor tries to follow the step reference on the $X$ axis, as illustrated in Fig. 3(b), Fig. 3(c), and Fig. 3(d). Fig. 3 also verifies that the tracking performance of ours is much better than that of INDI. Moreover, Fig. 4 shows that even with better control performance the control signals of ours are less noisy than that of INDI.

[1]Available at https://github.com/SihaoSun/INDI_Quadrotor_FTC and last accessed in December 2024.

TABLE III
CONTROL PARAMETERS OF THE INDI

| INDI Inner-Loop Controller | | | | |
|---|---|---|---|---|
| $k_{1,p}$ | $k_{1,d}$ | $k_{2,p}$ | $k_{2,d}$ | Time constant of the low-pass filter |
| 10 | 6 | 100 | 10 | 0.02 s |

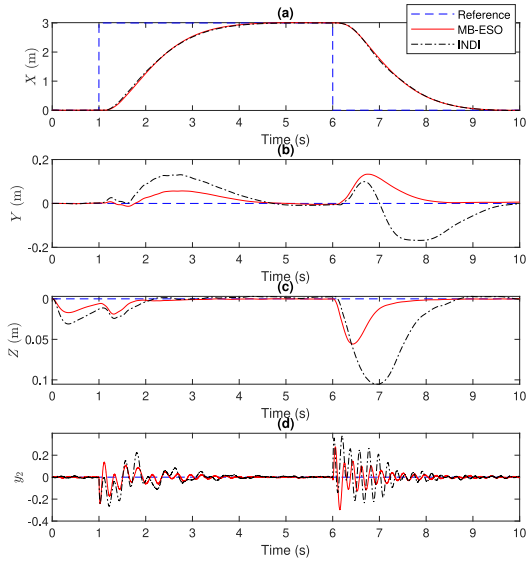


Fig. 3. Trajectory tracking comparison under windless condition.

To test the robustness of ours and INDI against model uncertainty and external disturbances with aggressive maneuvering, the maximum tilt angle of the quadrotor is changed to 60 degrees and a wind gust $(-15, 0, 0)$ m/s filtered by a low-pass filter with a transfer function $1/(4s+1)$, the same setting in the environment[1], is simulated continuously. The same reference trajectory as in Fig. 3 is used in the simulation. Fig. 5 shows the trajectory tracking results of ours and INDI simulating for 10 seconds. Both methods perform similarly during the first 7 seconds, when the wind strength remains relatively low. The position deviation from the reference is primarily caused by the outer-loop controller, which lacks the disturbance rejection capacity. After that, the quadrotor controlled by the INDI approach crashes. The robustness of INDI against the strong wind can be improved by using higher attitude control gains (*i.e.*, $k_{2,p}$ and $k_{2,d}$). However, this improvement is achieved by sacrificing the tracking performance, as illustrated in Fig. 6 with different $k_{2,p}=200$ and $k_{2,d}=30$.

## V. CONCLUSION

This letter proposes a novel FTC design based on the necessary and sufficient conditions for the existence of MB-ESO and the mismatched disturbance decoupling for a quadrotor experiencing two opposing rotor complete failures. Simulation results demonstrate that the proposed controller

Authorized licensed use limited to: University of Houston. Downloaded on February 18,2025 at 21:35:07 UTC from IEEE Xplore. Restrictions apply.

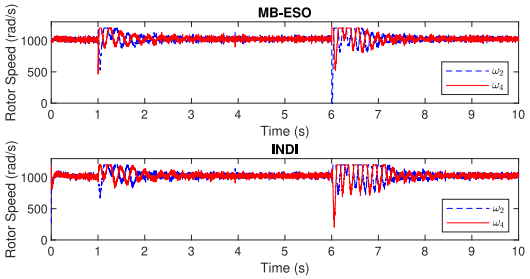


Fig. 4. Comparison of angular speed commands of rotor 2 and 4.

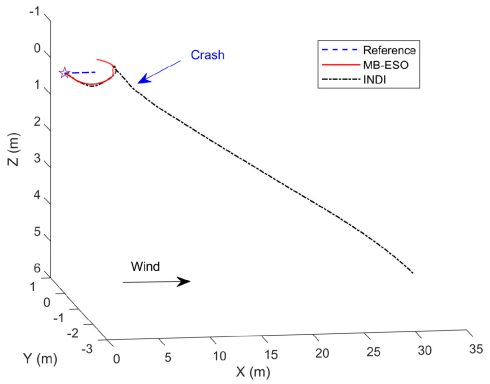


Fig. 5. 3-D trajectories of the quadrotor under strong wind via MB-ESO and INDI. The star represents the starting point.

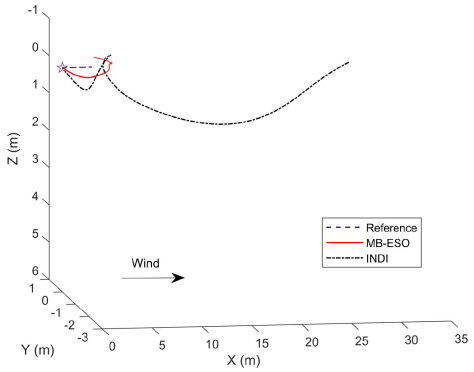


Fig. 6. 3-D trajectories of the quadrotor under strong wind via MB-ESO and INDI. The inner-loop control parameters, $k_{2,p}$ and $k_{2,d}$, of the INDI are changed to 200 and 30, respectively.

outperforms the well-known INDI against disturbances caused by significant aerodynamic effects in extreme conditions.

## REFERENCES

[1] A. Freddi, A. Lanzon, and S. Longhi, "A feedback linearization approach to fault tolerance in quadrotor vehicles," *IFAC Proc. Vol.*, vol. 44, no. 1, pp. 5413–5418, 2011.

[2] M. W. Mueller and R. D'Andrea, "Stability and control of a quadrocopter despite the complete loss of one, two, or three propellers," in *Proc. IEEE Int. Conf. Robot. Autom.*, 2014, pp. 45–52.

[3] S. Sun, L. Sijbers, X. Wang, and C. de Visser, "High-speed flight of quadrotor despite loss of single rotor," *IEEE Robot. Autom. Lett.*, vol. 3, no. 4, pp. 3201–3207, Oct. 2018.

[4] S. Sun, X. Wang, Q. Chu, and C. D. Visser, "Incremental nonlinear fault-tolerant control of a quadrotor with complete loss of two opposing rotors," *IEEE Trans. Robot.*, vol. 37, no. 1, pp. 116–130, Feb. 2021.

[5] F. Nan, S. Sun, P. Foehn, and D. Scaramuzza, "Nonlinear MPC for quadrotor fault-tolerant control," *IEEE Robot. Autom. Lett.*, vol. 7, no. 2, pp. 5047–5054, Apr. 2022.

[6] C. Ke, K. Cai, and Q. Quan, "Uniform fault-tolerant control of a Quadcopter with rotor failure," *IEEE/ASME Trans. Mechatronics*, vol. 28, no. 1, pp. 507–517, Feb. 2023.

[7] C. Ke, K.-Y. Cai, and Q. Quan, "Uniform passive fault-tolerant control of a quadcopter with one, two, or three rotor failure," *IEEE Trans. Robot.*, vol. 39, no. 6, pp. 4297–4311, Dec. 2023.

[8] M. W. Mueller and R. D'Andrea, "Relaxed hover solutions for multicopters: Application to algorithmic redundancy and novel vehicles," *Int. J. Robot. Res.*, vol. 35, no. 8, pp. 873–889, 2016.

[9] J. Han, "From PID to active disturbance rejection control," *IEEE Trans. Ind. Electron.*, vol. 56, no. 3, pp. 900–906, Mar. 2009.

[10] C. Wang, W. Li, and M. Liang, "Event-triggered prescribed performance adaptive fuzzy fault-tolerant control for quadrotor UAV with actuator saturation and failures," *IEEE Trans. Aerosp. Electron. Syst.*, early access, Aug. 23, 2024, doi: 10.1109/TAES.2024.3448404.

[11] Y. Guo, B. Jiang, and Y. Zhang, "A novel robust attitude control for quadrotor aircraft subject to actuator faults and wind gusts," *IEEE/CAA J. Automatica Sinica*, vol. 5, no. 1, pp. 292–300, Jan. 2018.

[12] Y. Du, P. Huang, Y. Cheng, Y. Fan, and Y. Yuan, "Fault tolerant control of a quadrotor unmanned aerial vehicle based on active disturbance rejection control and two-stage Kalman filter," *IEEE Access*, vol. 11, pp. 67556–67566, 2023.

[13] J. Chen, Z. Gao, Y. Hu, and S. Shao, "A general model-based extended state observer with built-in zero dynamics," 2023, *arXiv:2208.12314*.

[14] J. Yang, S. Li, and W. Chen, "Nonlinear disturbance observer-based control for multi-input multi-output nonlinear systems subject to mismatching condition," *Int. J. Control*, vol. 85, no. 8, pp. 1071–1082, 2012.

[15] A. Isidori, *Nonlinear Control Systems*, 3rd ed. London, U.K.: Springer, 1995. [Online]. Available: https://link.springer.com/book/10.1007/978-1-84628-615-5

[16] Z. Gao, "Scaling and bandwidth-parameterization based controller tuning," in *Proc. Amer. Control Conf.*, 2003, pp. 4989–4996.

[17] W. Bai, S. Chen, Y. Huang, B. Guo, and Z. Wu, "Observers and observability for uncertain nonlinear systems: A necessary and sufficient condition," *Int. J. Robust Nonlinear Control*, vol. 29, no. 10, pp. 2960–2977, 2019.

[18] M. Hou and P. Muller, "Disturbance decoupled observer design: A unified viewpoint," *IEEE Trans. Autom. Control*, vol. 39, no. 6, pp. 1338–1341, Jun. 1994.

[19] J. C. Willems and C. Commault, "Disturbance decoupling by measurement feedback with stability or pole placement," *SIAM J. Control Optim.*, vol. 19, no. 4, pp. 490–504, 1981.

Authorized licensed use limited to: University of Houston. Downloaded on February 18,2025 at 21:35:07 UTC from IEEE Xplore. Restrictions apply.